A Novel Fuzzy-Logic Controlled Tri-PortConverter Fed SRM Drive for EV Application Powered by Solar-PV System

1M.Venkateswarlu, 2A.Raghavendrudu, 3V.Yogeswar Yadav, 4K.Vamsidhar Reddy, 5P.Uday Kumar,
1 Assistant Professor, 2,3,4,5 B-tech students Scholar
1,2, 3, 4, 5 Department of Electrical and electronics engineering,
1, 2, 3, 4, 5 G. Pullaiah College of Engineering and Technology, Nandikotkur Rd,
Near Venkayapalle, Pasupala Village, Kurnool, Andhra Pradesh, 518002.

Abstract-Electric vehicle technology is becoming increasingly important as it takes care of the environmental issues related to ICE vehicle and reduces the dependency on fossil fuels. Electric vehicle being greatly dependent on the limited electrical energy provided by a battery, the power flow efficiency is very important in this context. Switched reluctance motors (SRMs) are one of promised motors for EV applications. In order to extend the EVs' driving miles, the use of photovoltaic (PV) panels on the vehicle helps decrease the reliance on vehicle batteries. Based on phase winding characteristics of SRMs, a tri-port converter is proposed in this work to control the energy flow between the Solar-PV panel, battery and SRM. Six operating modes are presented, four of which are developed for driving and two for standstill on-board charging. In the driving modes, the energy decoupling control for maximum power point tracking (MPPT) of the PV panel and speed control of the SRM are realized. In the standstill charging modes, a grid-connected charging topology is developed without a need for external hardware. When the PV panel directly charges the battery, a multi-section charging control strategy is used to optimize energy utilization.

The another objective is to regulate steady-state error in speed by using PI controller, this controller is un-popular due to tuning issues, to overcome this issues a new intelligent fuzzy-logic controller is adopted for achieving good performance. The proposed intelligent Fuzzy control schemes are highly used in several applications, in that Fuzzy controller has been greatly recognized due to enhanced performance over the classical PI controller.Simulation results based on Mat lab/Simulink prove the effectiveness of the proposed fuzzy-logic controller driven tri-port converter, which has potential economic implications to improve the market acceptance of EVs.

Index Terms—Electric vehicles, photo voltaic (PV), power flow control, switched reluctance motors (SRMs), tri-port converter.

1. INTRODUCTION

Photovoltaic Generators (PV) provide a clean and unlimited source of energy. As part of an ongoing project on low-cost PVpowered Electrical Vehicles, a control system is evaluated here for a specific configuration, based on PV panels that power a Switched Reluctance Motor, using independent controllers for maximizing the power supply and optimizing the operation of the motor [1-3]. In this paper the Simulink model for the speed control of switched reluctance motor is carried out by using different speed controllers. The Simulink models is designed for P, PI &Fuzzy logic controller separately and their performance result is been compared [4-5]. The Switched Reluctance Motor is an electric motor which runs by a reluctance torque. For industrial application very high speed of 50,000 rpm motor is used. The speed controllers applied here are based on conventional P& PI Controller and the other one is AI based Fuzzy Logic Controller [6-7].

The PI Controller proportional integral controller) is a most special case of the PID controller in which the derivative of the error is not being used. Fuzzy logic controller is a most intelligent controller which uses a fuzzy logic to process the input. Fuzzy logic is a many valued logic which is much like a human reasoning. In the industrial control FLC has various applications, particularly where this conventional control design techniques are very difficult to apply. A comprehensive reviews has done for SRM machine modeling, design and simulation and analysis and control [8-10].

Switched Reluctance Motor (SRM) has undergone fast growth in airspace starter/generator system, hybrid electric vehicles, washing machines, and industrial automation applications over the most recent decades [11]. The main reason behind this is SRM has simple, robust construction and reliable operation. So it can be used as a drive in vibrating and high temperature areas. In addition the cost of the SRM is low and the size of the motor is little and lower weight [12]. However the SRM is a nonlinear motor because it operates in saturation to produce maximum output torque and the developed torque is a nonlinear function of both rotor position and phase current. So it is not advisable to use conventional PID controller to control the speed of switched reluctance motor [13]. Fuzzy logic controller (FLC) one of the intelligent control technique, is used in this work. FLC

uses human problem solving methodology to control the speed of non-linear system and the performance of FLC is also good. FLC provides a proper approach for representing, influencing, and executing a human's heuristic knowledge about how to control a system [14]. Application of FLC in control nonlinear, parameter disparity, structure variation and transfer function unknown system shows the suitability of FLC to control the speed of SRM. The simulation was carried out with PID controller and FLC the results obtained are analyzed to test the performance of fuzzy logic controller. The FLC based speed control technique for SRM shows better performance [15].

II. Topology and Operational Modes

A. Proposed topology and working modes

The proposed Tri-port topology has three energy terminals, PV, battery and SRM. They are linked by a power converter which consists of four switching devices (S0~S3), four diodes (D0~D3) and two relays, as shown in Fig.1. [10]. By controlling relays J1 and J2, the six operation modes are supported, as shown in Fig. 3; the corresponding relay actions are illustrated in Table I. In mode 1, PV is the energy source to drive the SRM and to charge the battery. In mode 2, the PV and battery are both the energy sources to drive the SRM. In mode 3, the PV is the source and the battery is idle. In mode 4, the battery is the driving source and the PV is idle. In mode 5, the battery is charged by a single-phase grid while both the PV and SRM are idle. In mode 6, the battery is charged by the PV and the SRM is idle.
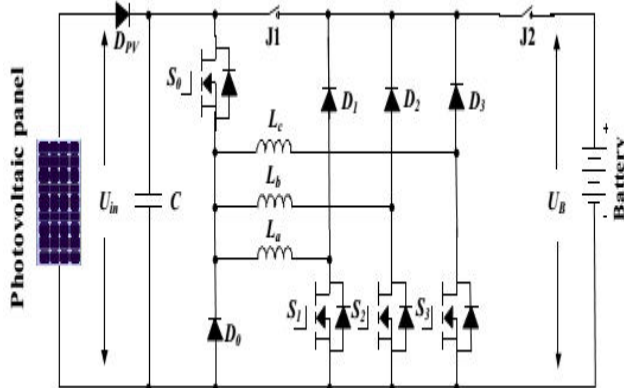
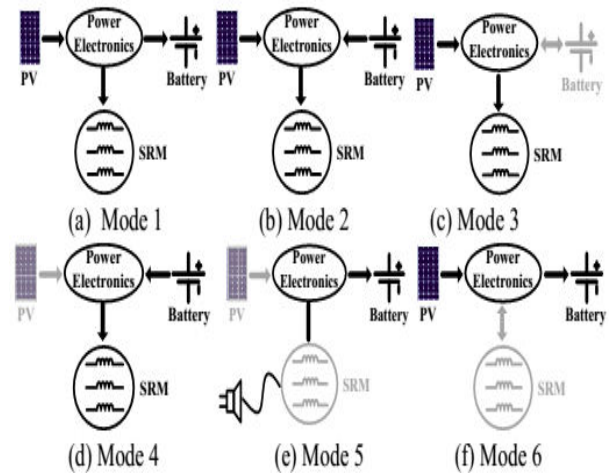Fig.1. the proposed Tri-port topology for PV-powered SRM drive.

Fig.2. Six operation modes of the proposed Tri-port topology.

TABLE 1. J1 and J2 Actions under Different Modes

| Mode	J1 and J2
1	J1 turn-off; J2 turn-on
2	J1 and J2 turn-on
3	J1 turn-on; J2 turn-off
4	J1 and J2 turn-on
5	J1 and J2 turn-on
6	J1 turn-off; J2 turn-on

B. Driving modes

Operating modes 1~4 are the driving modes to provide traction drive to the vehicle.

(1) Mode 1

At light loads of operation, the energy generated from the PV is more than the SRM needed; the system operates in mode 1. The corresponding operation circuit is shown in Fig.3 (a), in which relay J1 turns off and relay J2 turns on. The PV panel energy feed the energy to SRM and charge the battery; so in this mode, the battery is charged in EV operation condition.
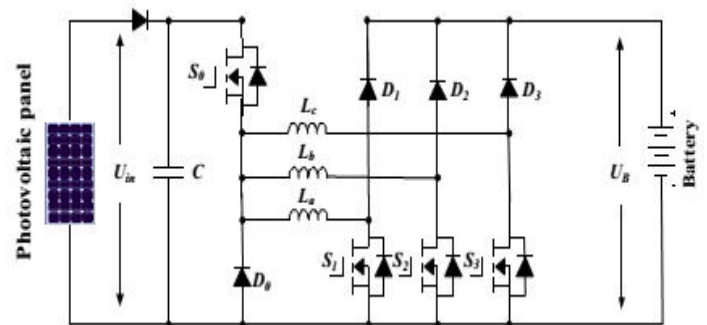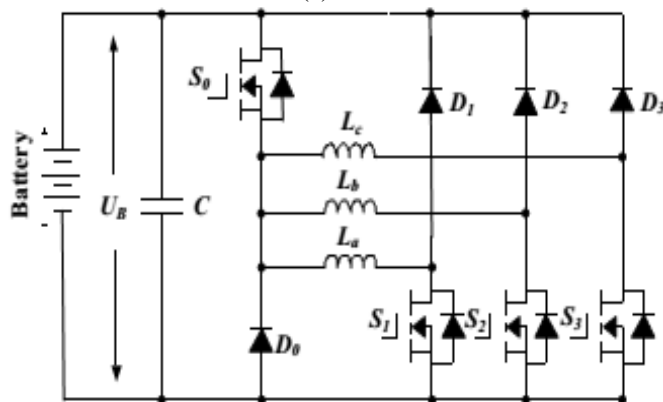
(a).Operation circuit under mode 1
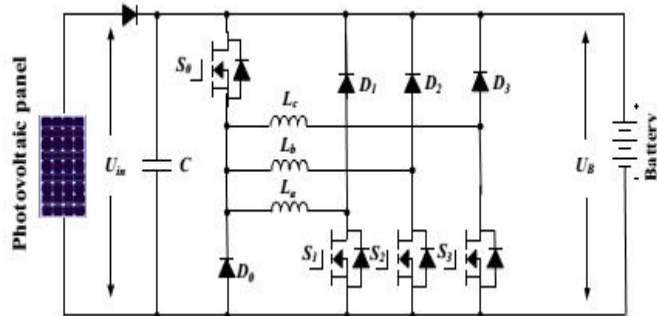
(b)
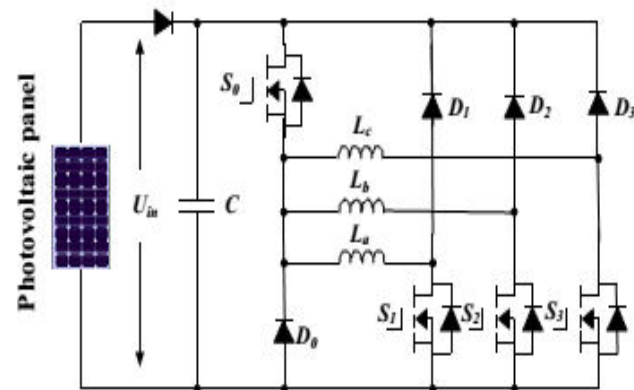
(c)

(d).Operation circuit under mode 4
Fig.3.The equivalent circuits under driving modes.

(2) Mode 2

When the SRM operates in heavy load such as uphill driving or acceleration, both the PV panel and battery supply power to the SRM. The corresponding operation circuit is shown in Fig. 3(b), in which relay J1 and J2 are turned on.

(3) Mode 3

When the battery is out of power, the PV panel is the only energy source to drive the vehicle. The corresponding circuit is shown in Fig. 3(c). J1 turns on and J2 turns off.

(4) Mode 4

When the PV cannot generate electricity due to low solar irradiation, the battery supplies power to the SRM. The corresponding topology is illustrated in Fig. 3(d). In this mode, relay J1 and J2 are both conducting.

C. Battery charging modes

Operating modes 5 and 6 are the battery charging modes.

(5) Mode 5

When PV cannot generate electricity, an external power source is needed to charge the battery, such as AC grid. The corresponding circuit is shown in Fig. 4(a). J1 and J2 turns on. Point A is central tapped of phase windings that can be easily achieved without changing the motor structure. One of the three phase windings is split and its midpoint is pulled out, as shown in Fig. 4(a). Phase windings La1 and La2 are employed as input filter inductors. These inductors are part of the drive circuit to form an AC-DC rectifier for grid charging.

(6) Mode 6

When the EV is parked under the sun, the PV can charge the battery. J1 turns off; J2 turns on. The corresponding charging circuit is shown in Fig.4 (b).
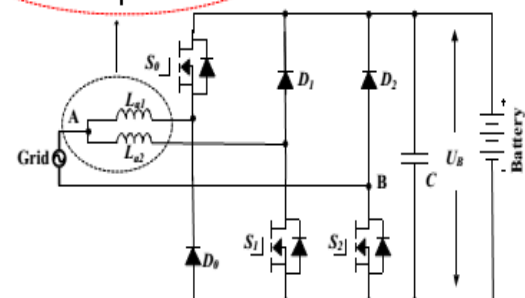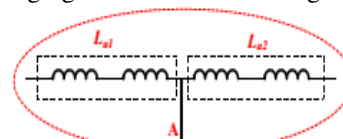
(a) Grid charging mode
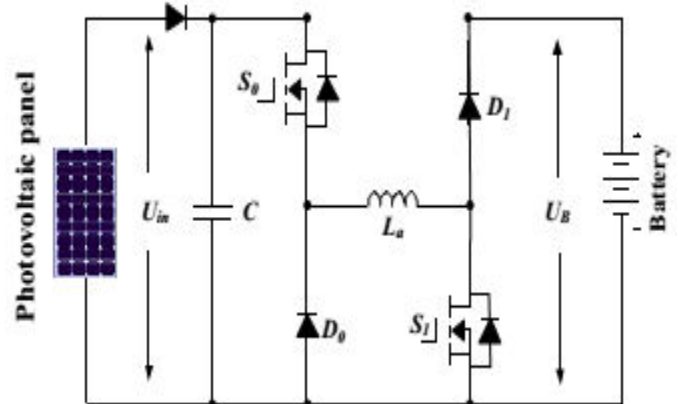
(b) PV source charging mode
Fig.4 Equivalent circuits of charging condition modes

III. Control Strategy under Different Modes

In order to make the best use of solar energy for driving the EV, a control strategy under different modes is designed.

A. Single source driving mode

According to the difference in the power sources, there are PV-driving; battery-driving and PV and battery parallel fed source. In a heavy load condition, the PV power cannot support the EV, mode 2 can be adopted to support enough energy and make full use of solar energy. Fig. 5(a) shows the equivalent power source; the corresponding PV panel working points is illustrated in Fig.5 (b). Because the PV is paralleled with the battery, the PV panel voltage is clamped to the battery voltage UB. In mode 2, there are three working states: winding excitation, energy recycling and freewheeling states, as shown in Fig.6. Modes 3 and 4 have similar working states to mode 2. The difference is that the PV is the only source in mode 3 while the battery is the only source in mode 4.

(a) Compound power source   (b) Working point of the PV
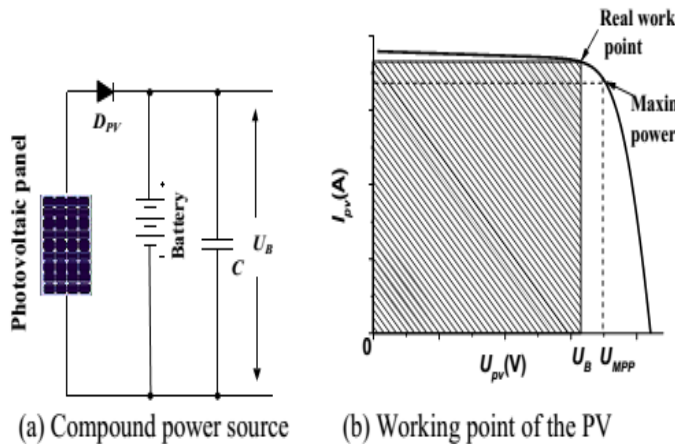
Fig.5. Power supply at mode 2

(a) Winding excitation state   (b) Energy recycling state
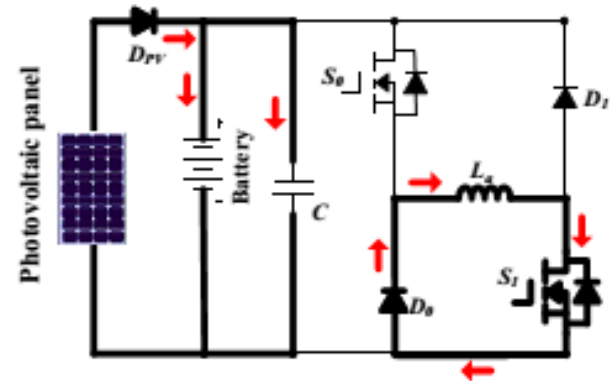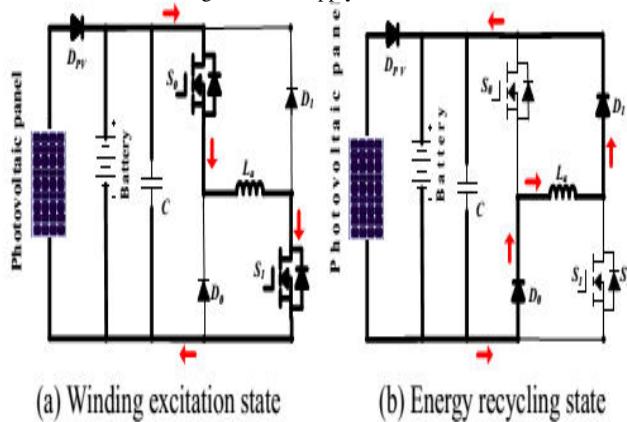
(c) Freewheeling state

Fig.6. Working states at mode 2

Neglecting the voltage drop across the power switches and diodes, the phase voltage is given by

$$U_{in} = R_k i_k + \frac{d\psi(i_k, \theta_r)}{dt}$$
$$= R_k i_k + L_k \frac{di_k}{dt} + i_k \omega_r \frac{dL_k}{d\theta_r}, \quad k = a,b,c \quad (1)$$

where Uin is the DC-link voltage, k is phase a, b, or c, Rk is the phase resistance, ik is the phase current, Lk is the phase inductance, θ_r is the rotor position, $\psi(i_k, \theta_r)$ is the phase flux linkage depending on the phase current and rotor position, and ω_r is the angular speed. The third term in Eq.1 is the back electromotive force (EMF) voltage given by

$$e_k = i_k \omega_r \frac{dL_k}{d\theta_r} \quad (2)$$

Hence, the phase voltage is found by

$$U_k = R_k i_k + L_k \frac{di_k}{dt} + e_k \quad (3)$$

In the excitation region, turning on S0 and S1 will induce a current in phase a winding, as show in Fig.6 (a). Phase a winding is subjected to the positive DC bus voltage.

$$+U_{in} = R_k i_k + L_k \frac{di_k}{dt} + e_k \quad (4)$$

When S0 is off and S1 is on, the phase current is in a freewheeling state in a zero voltage loop, as shown in Fig.6(c), the phase voltage is zero.

$$0 = R_k i_k + L_k \frac{di_k}{dt} + e_k \quad (5)$$

In the demagnetization region, S0 and S1 are both turned off, and the phase current will flow back to the power supply, as show in Fig.6 (b). In this state, the phase winding is subjected to the negative DC bus voltage, and the phase voltage is

$$-U_{in} = R_k i_k + L_k \frac{di_k}{dt} + e_k$$

(6)

In single source driving mode, the voltage-PWM control is employed as the basic scheme, as illustrated in Fig.7. According to the given speed ω*, the voltage-PWM control is activated at speed control.
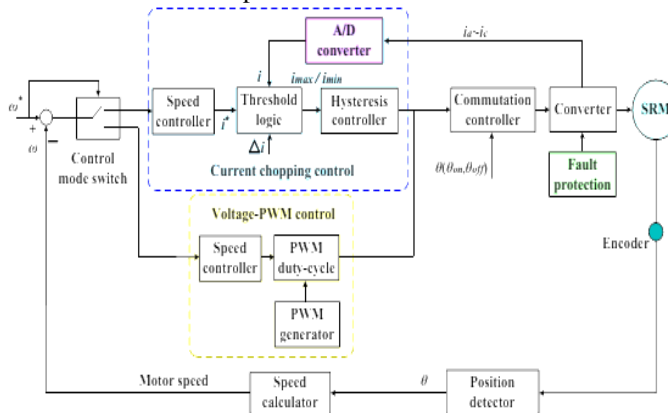
Fig 7. SRM control strategy under single source driving mode.

B. Driving-charging hybrid control strategy

In the driving-charging hybrid control, the PV is the driving source and the battery is charged by the freewheeling current, as illustrated in drive mode 1. There are two control objectives: maximum power point tracking (MPPT) of the PV panel and speed control of the SRM.

The dual-source condition is switched from a PV-driving mode. Firstly, the motor speed is controlled at a given speed in mode 3. Then, J2 is tuned on and J1 is off to switch to mode 1. By controlling the turn-off angle, the maximum power of PV panel can be tracked.

There are three steady working states for the dual-source mode (mode 1), as shown in Fig.8. In Fig. 8(a), S0 and S1 conduct, the PV panel charges the SRM winding to drive the motor; In Fig. 8(b), S0 and S1 turn off; and the battery is charged with freewheeling current of the phase winding.

(a)   Winding exciting state

(b)   Battery charging state
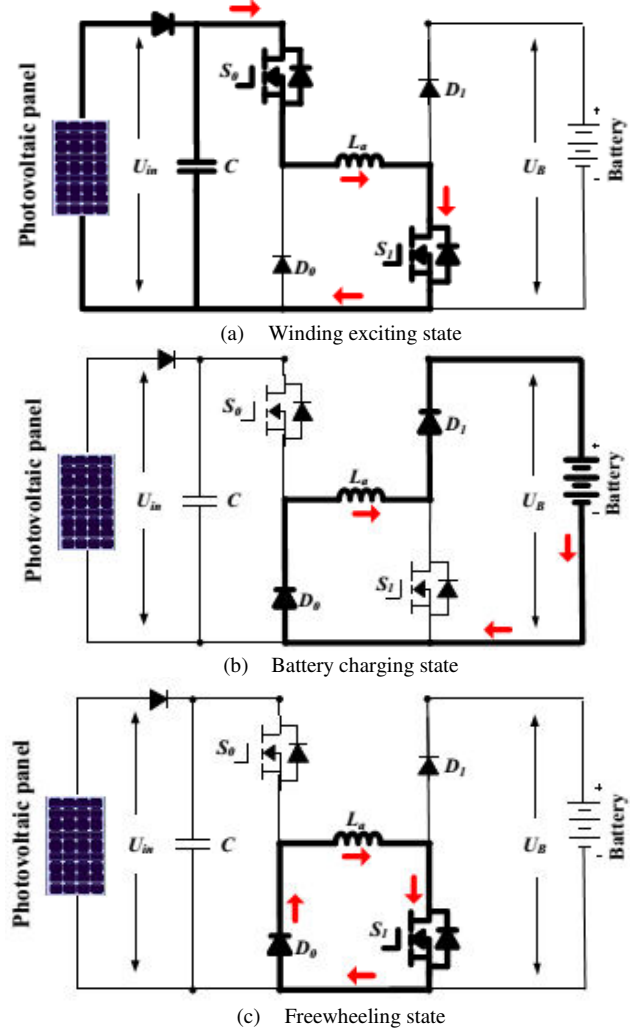
(c)   Freewheeling state
Fig.8 Mode 1 working states

Fig.9 is the control strategy under driving-charging mode. In Fig.9, θon is the turn on angle of SRM; θoff is the turn-off angle of SRM. By adjusting turn-on angle, the speed of SRM can be controlled; the maximum power point tracking of PV panel can be achieved by adjusting turn-off angle, which can control the charging current to the battery.
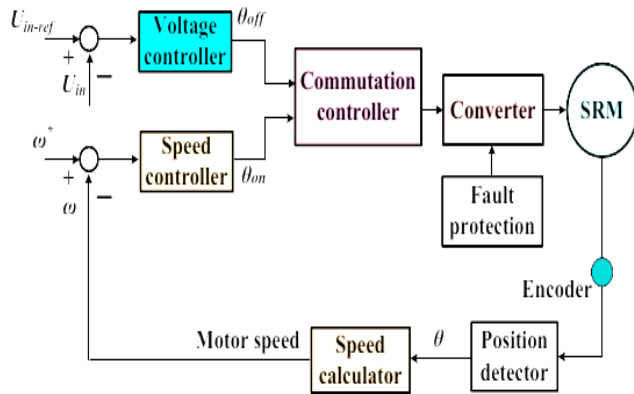
Fig.9. Control strategy under driving-charging mode (mode 1)

(a)   Grid charging state 1 (Ugrid>0)

C. Grid-charging control strategy

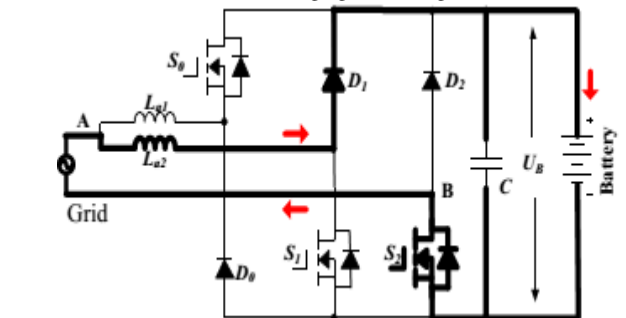   The proposed topology also supports the single-phase grid charging. There are four basic charging states and S0 is always turned off. When the grid instantaneous voltage is over zero, the two working states are presented in Fig.10 (a) and (b). In Fig.10 (a), S1 and S2 conduct, the grid voltage charges the phase winding La2, the corresponding equation can be expressed as Eq.7; In Fig.10.(b), S1 turns off and S2 conducts, the grid is connected in series with phase winding to charges the battery, the corresponding equation can be expressed as Eq.8.

$$U_{grid} = L_{a2} \cdot \frac{di_{grid}}{dt} \tag{7}$$

$$U_B - U_{grid} = L_{a2} \cdot \frac{di_{grid}}{dt} \tag{8}$$

(b) Grid charging state 2 (Ugrid>0)

When the grid instantaneous voltage is below zero, the two working states are presented in Fig. 10(c) and (d). In Fig.10.(c), S1 and S2 conduct, the grid voltage charges the phase winding La1 and La2, the corresponding equation can be expressed as Eq. (9); In Fig.10(d), S1 keeps conducing and S2 turns off, the grid is connected in series with phase winding La1 and La2 to charges the battery, the corresponding equation can be expressed as Eq.10.

$$U_{grid} = \frac{L_{a1} + L_{a2}}{L_{a1} \cdot L_{a2}} \cdot \frac{di_{grid}}{dt} \tag{9}$$

$$-U_B - U_{grid} = \frac{L_{a1} + L_{a2}}{L_{a1} \cdot L_{a2}} \cdot \frac{di_{grid}}{dt} \tag{10}$$

(c)   Grid charging state 3 (Ugrid<0)
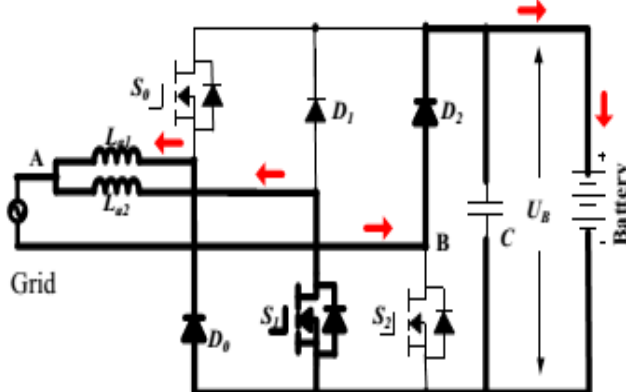
(d) Grid charging state 4 (Ugrid<0)

Fig.10. Mode 5 charging states

In Fig.11.Ugrid is the grid voltage; by the phase lock loop (PLL), the phase information can be got; Iref_grid is the given amplitude of the grid current. Combining sinθ and Iref_grid, the instantaneous grid current reference iref_grid can be calculated. In this mode, when Ugrid> 0, the inductance is La2; when Ugrid< 0, the inductance is paralleled La1 and La2; in order to adopt the change in the inductance, hysteresis control is employed to realize grid current regulation. Furthermore, hysteresis control has excellent loop performance, global stability and small phase lag that makes grid connected control stable.

(a)   Phase inductance charging
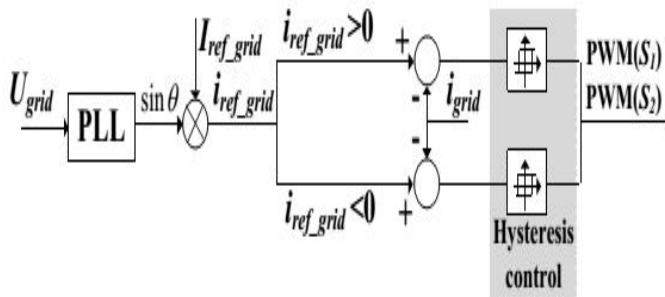
Fig.11. Grid-connected charging control (Mode 5).

D. PV-fed charging control strategy

In this mode, the PV panel charges the battery directly by the driving topology. The phase windings are employed as inductor; and the driving topology can be functioned as interleaved Buck boost charging topology. For one phase, there are two states, as shown in Fig. 12(a) and (b). When S0 and S1 turn on, the PV panel charges phase inductance; when S0 and S1 turns off, the phase inductance discharges energy to battery. According to the state-of-charging (SoC), there are three stages to make full use of solar energy and maintain battery healthy condition, as illustrated in Fig.12 (c). During stage 1, the corresponding battery SoC is in 0~SoC1, the battery is in extremely lack energy condition, the MPPT control strategy is employed to make full use of solar energy. During stage 2, the corresponding battery SoC is in SoC1~ SoC2, the constant voltage control is adapted to charging the battery. During stage 3, the corresponding battery SoC is in SoC2~1, the micro current charging is adapted. In order to simplify the control strategy, constant voltage is employed in PV panel MPPT control.

(b)   Battery charging

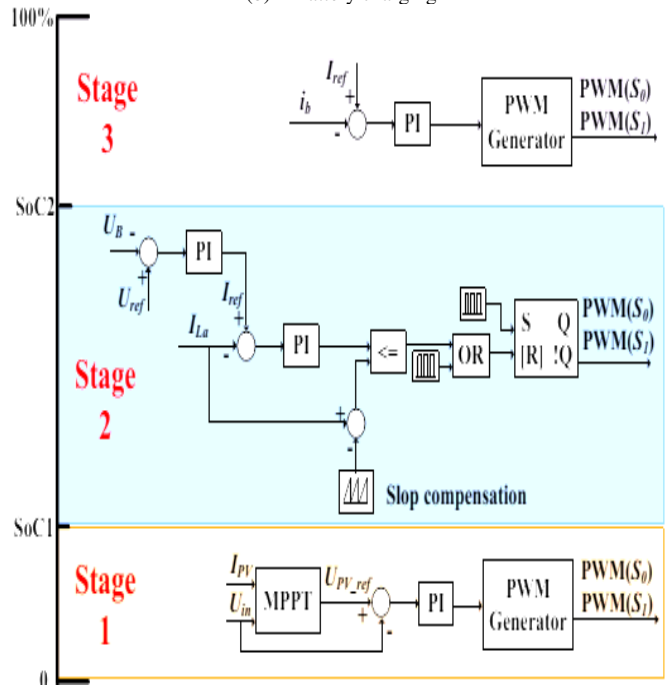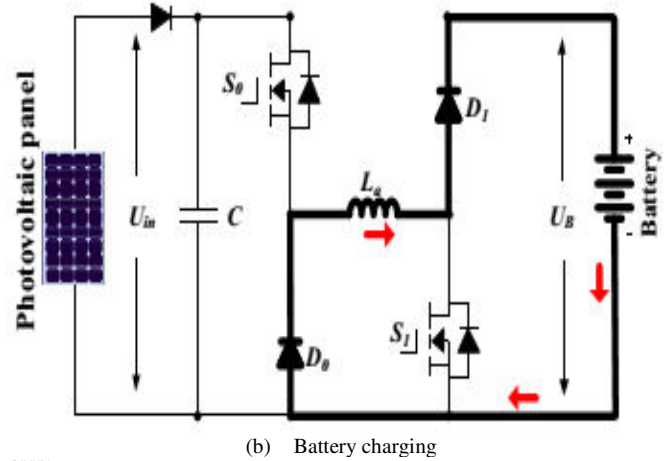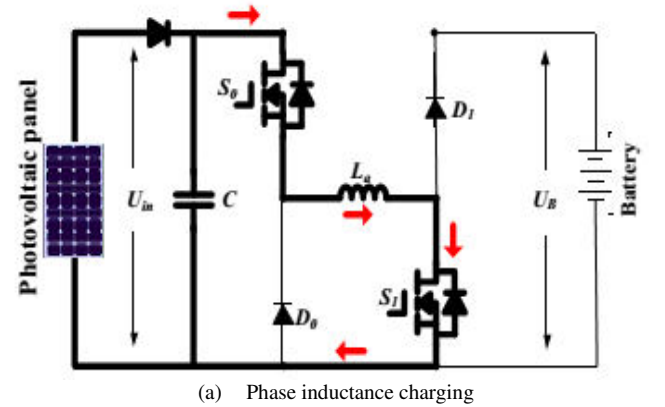(c) Charging control strategy.
Fig.12 Mode 6 charging states and control strategy.

VII. DESIGN OF A FUZZY CONTROLLER

The trouble with respect to the PI controller gain is the adjusting of the controller in order to accomplish the ideal activity of the undertaking. The significant disadvantage of the PI controller is confronted when the procedure is nonlinear and furthermore when the framework is having motions. Thinking about every one of these actualities, a fluffy rationale controller was actualized. A fluffy controller can work in direct and additionally in nonlinear structure parameters. Fluffy Logic requires some numerical parameters with the end goal to work, for example, what is viewed as huge mistake and huge rate-of-progress of blunder, yet correct estimations of these numbers are normally not basic except if extremely responsive execution is required in which case experimental tuning would decide them.
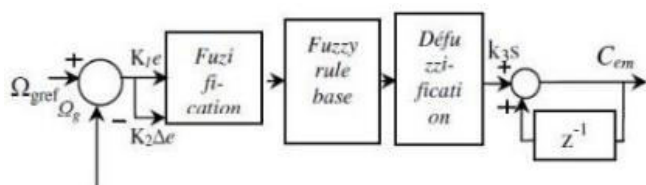
Fig.13 Fuzzy Logic Controller

FL requires some numerical parameters with the end goal to work, for example, what is viewed as noteworthy mistake and huge rate-of-change of-blunder, yet correct estimations of these numbers are normally not basic except if extremely responsive execution is required in which case exact tuning would decide them. For instance, a temperature control framework could utilize a solitary temperature criticism sensor whose information is subtracted from the direction flag to process "blunder" and after that time-separated to yield the mistake incline or rate-of progress of-blunder, in the future called "blunder dab".

MATLAB/SIMULATION RESULTS
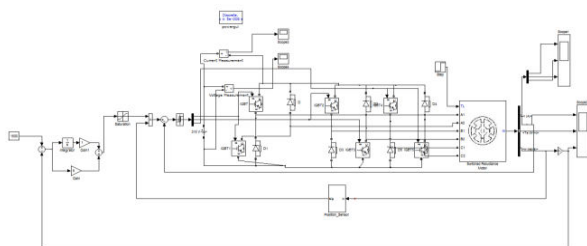
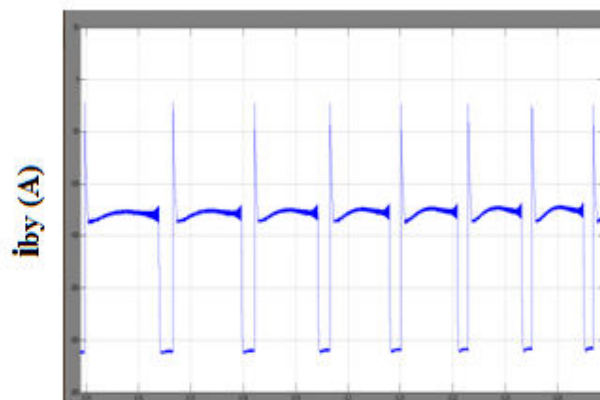Fig.14 Matlab/simulinkcircuit for SRM drive

model diagram

(a)

(b)
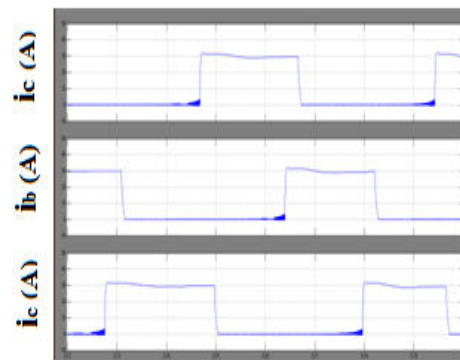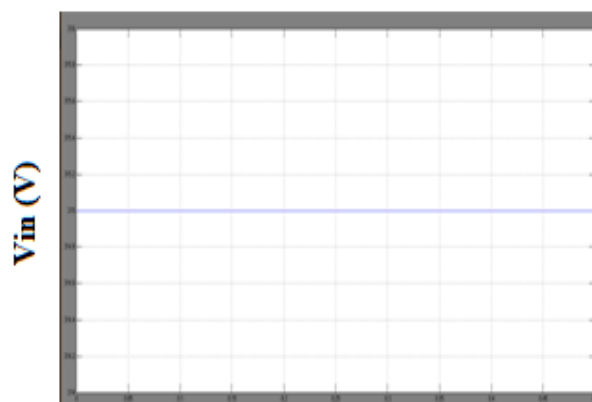
(c)

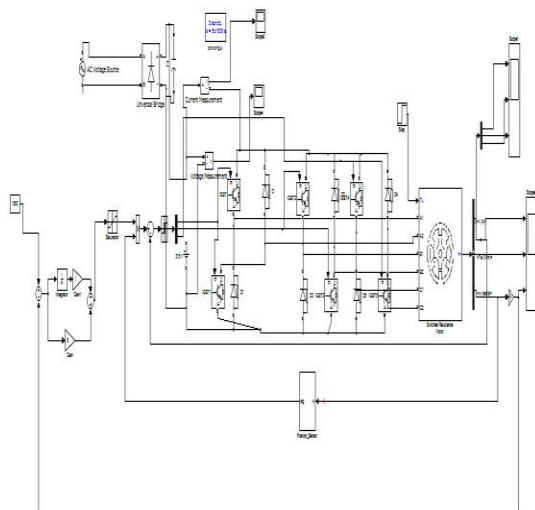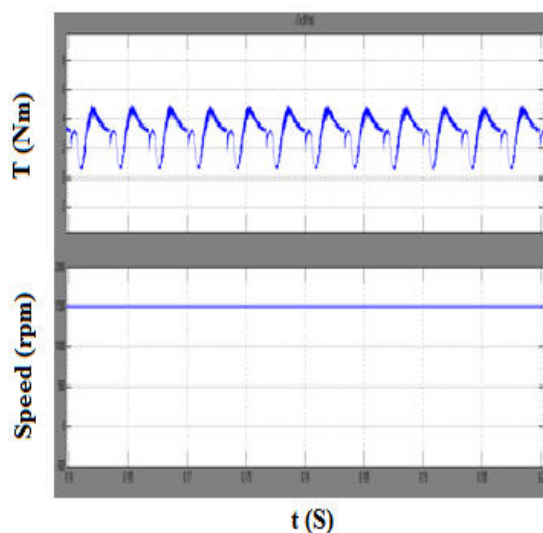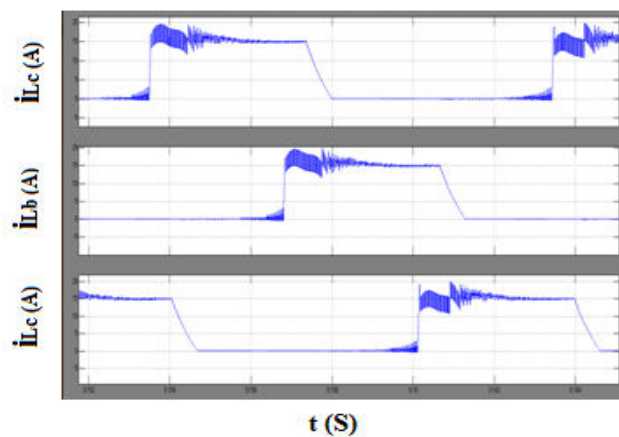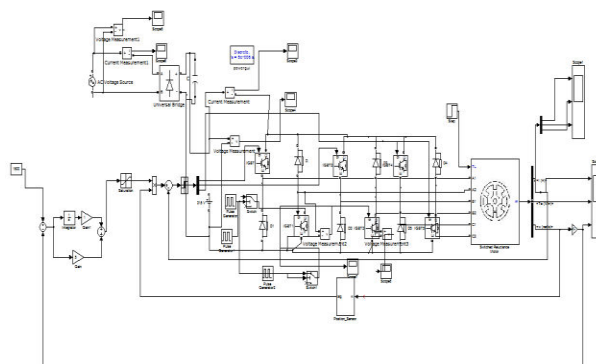Fig 15 Simulation results of driving-charging
mode (mode 1)

(b) Simulation results of single source driving
mode (modes 3 and 4)

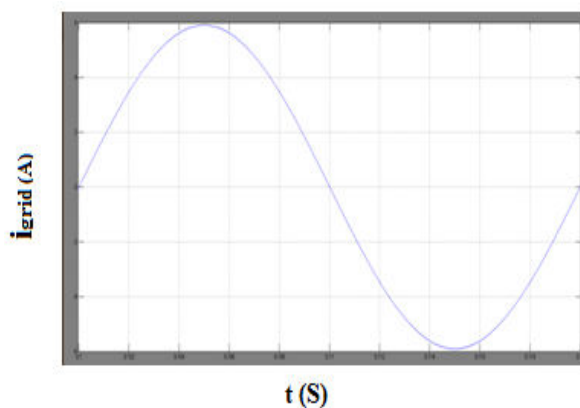Fig.17 Simulation results for driving conditions
at modes 1, 3 and 4.

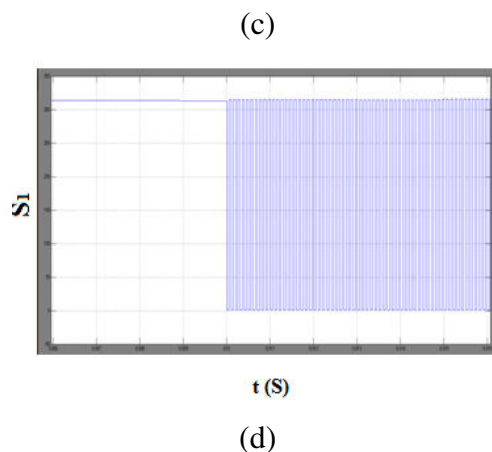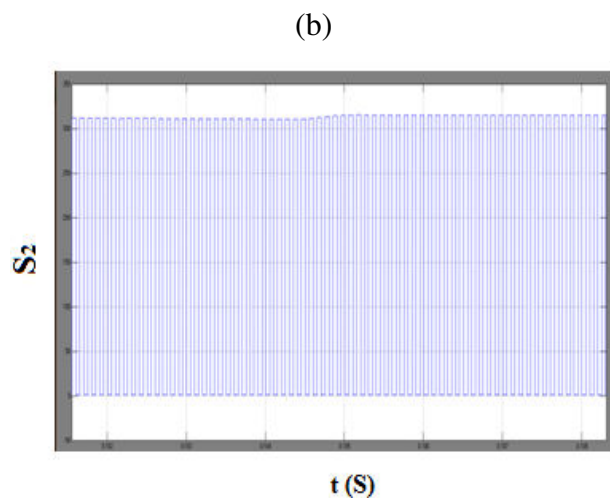Fig.16 Matlab/simulinkcircuit for SRM drive
model diagram

Fig.18 Matlab/simulinkcircuit for SRM drive
model diagram

(a)

(a)

(b)

Fig.20 Matlab/simulinkcircuit for PV-powered

SRM drive model diagram

(c)

(a)

(d)
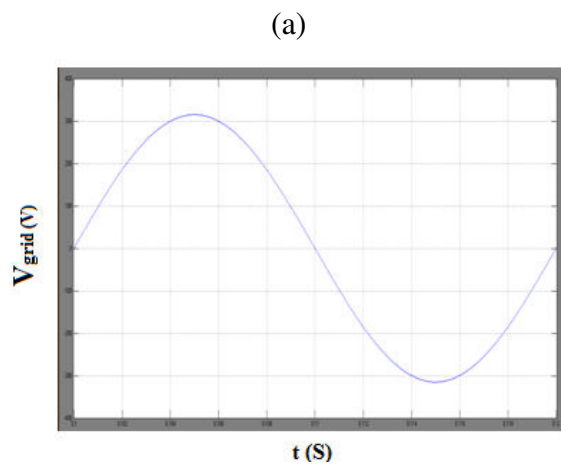
Fig.19. Grid charging (mode 5)

(b)

(c)
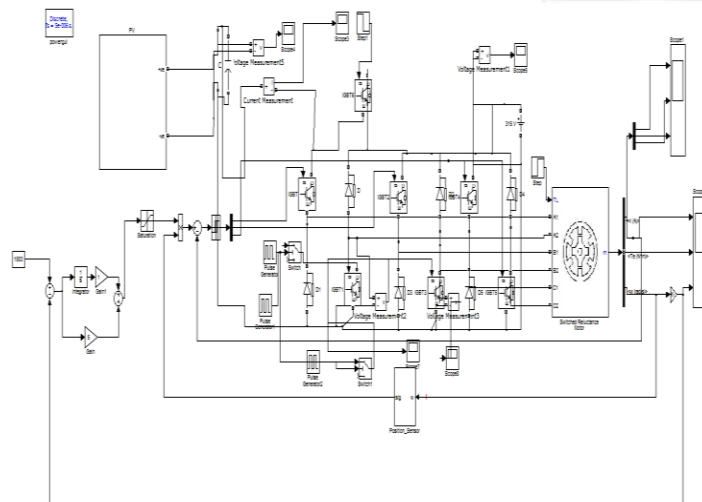
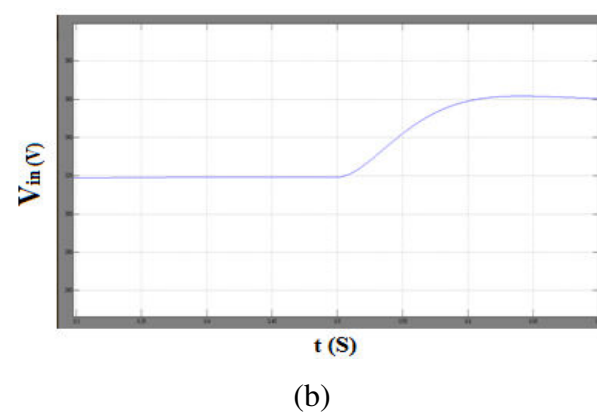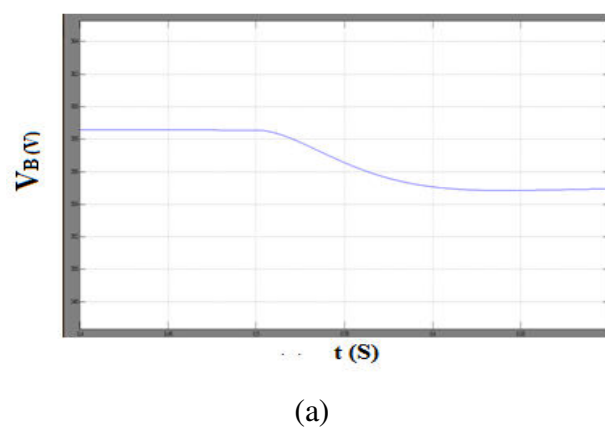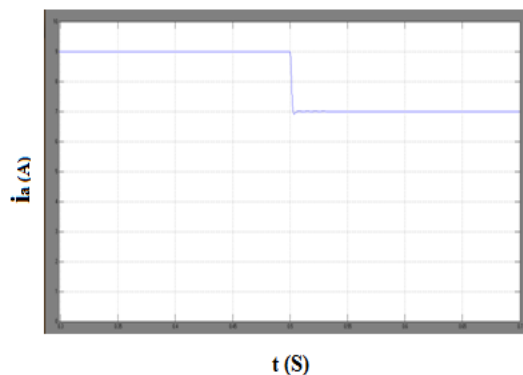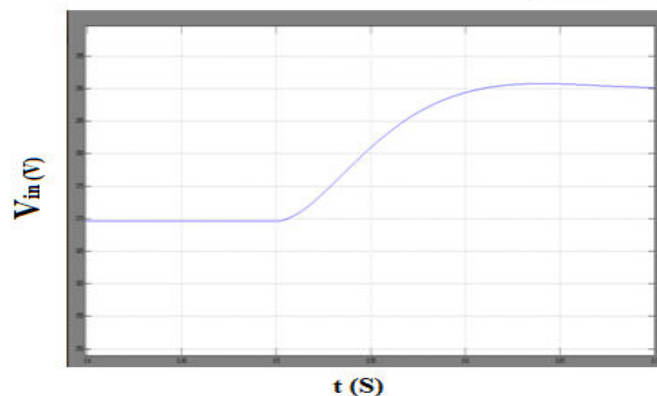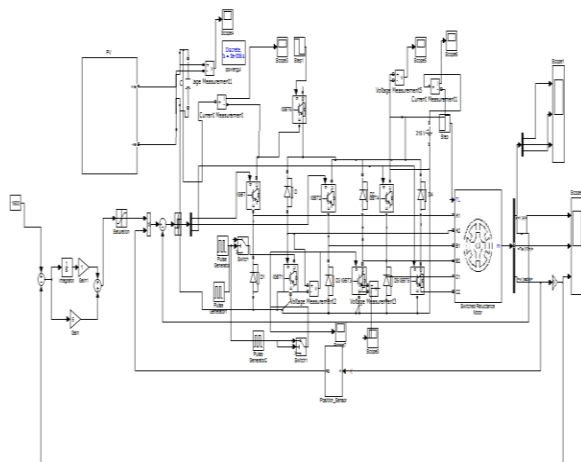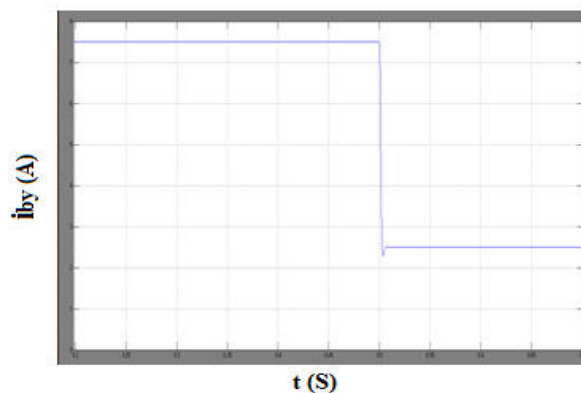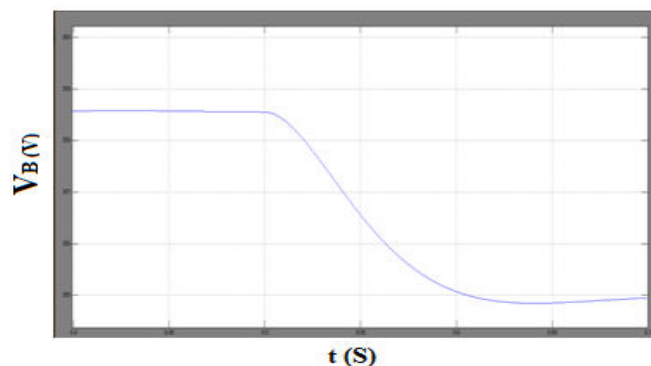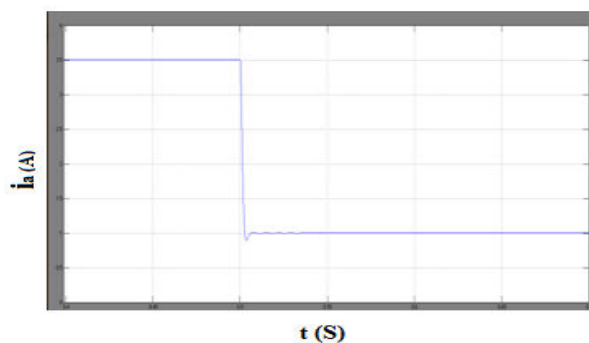Fig.21 PV charging mode 6 (stage 1 to stage 2)

(b)

Fig.22 Matlab/simulinkcircuit for PV-powered

SRM drive model diagram

(c)

(a)

(a) PV charging mode 6 (stage 2 to stage 3)
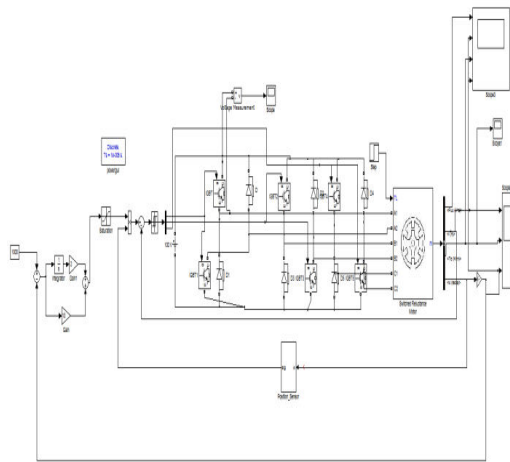
Fig.23 Simulation results for charging modes.

Fig.24 Matlab/simulinkcircuit for SRM drive

model diagram With PI controller

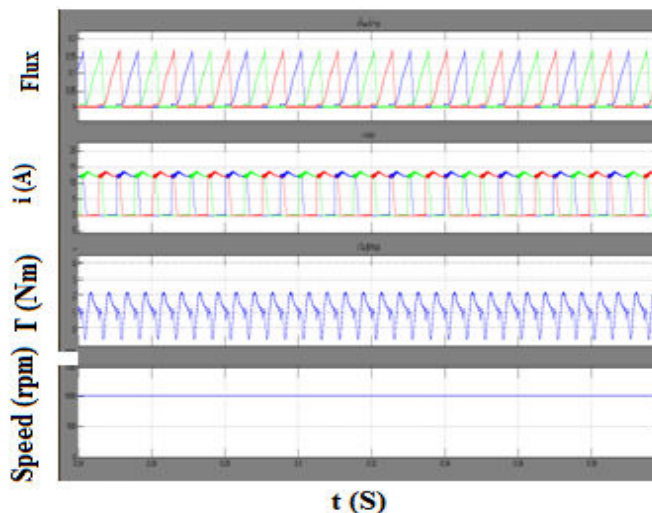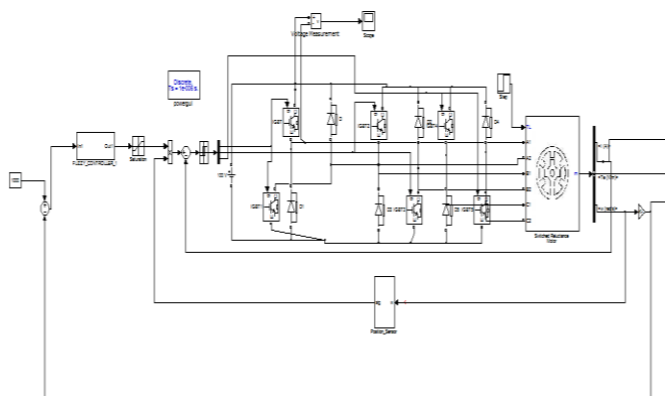Fig.25 Flux, Current, Speed and Torque

Fig.26 Matlab/simulinkcircuit for SRM drive

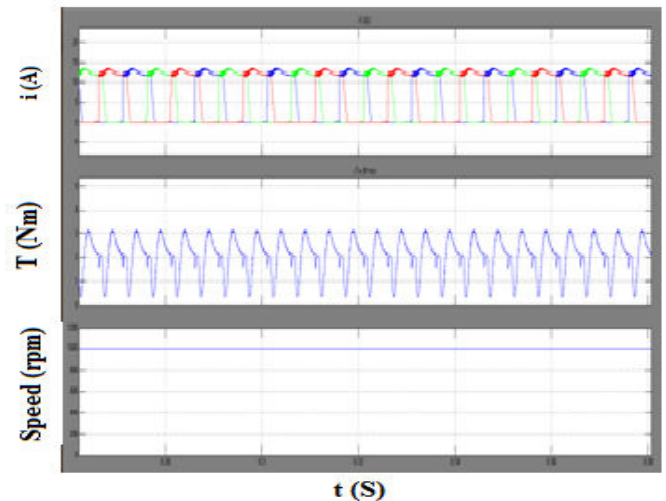model diagram With Fuzzy controller

Fig.27 Current, Speed and Torque of SRM

CONCLUSION

Since PV-fed EVs are a greener and more sustainable technology than conventional ICE vehicles, this work will provide a feasible solution to reducing the total costs and CO_2 emissions of electrified vehicles. Furthermore, the proposed technology may also be applied to similar applications such as fuel cell powered EVs. Fuel cells have a much higher power density and are thus better suited for EV applications. In this work the SRM dynamicperformance is implemented by usingMATLAB/Simulink. In conventional methods the speed control of SRM motor is concluded by P, PI. Here it is executed with Fuzzy Logic Controller. Fuzzy Logic Controller gives the required output than the other controllers. In this proposed method the fuzzy logic controller ensure excellent reference tracking of switched reluctance motor drives. This fuzzy logic controller gives the best speed tracking without overshoot andenhances the speed regulation.

REFERENCES

[1] A. Emadi, L. Young-Joo, K. Rajashekara, "Power electronics and motor drives in electric, hybrid electric, and plug-in hybrid electric vehicles," IEEE Trans. Ind. Electron., vol. 55, no. 6, pp. 2237-2245, Jun. 2008.
[2] B. l. K. Bose, "Global energy scenario and impact of power electronics in 21st century," IEEE Trans. Ind. Electron., vol. 60, no. 7, pp. 2638-2651, Jul. 2013.
[3] J. de Santiago, H. Bernhoff, B. Ekergård, S. Eriksson, S. Ferhatovic, R. Waters, and M. Leijon,"Electrical motor drivelines in commercial allelectric vehicles: a review," IEEE Trans. Veh. Technol., vol. 61, no. 2, pp. 475-484, Feb. 2012.

[4] Z. Amjadi, S. S. Williamson, "Power-electronics-based solutions for plugin hybrid electric vehicle energy storage and management systems," IEEE Trans. Ind. Electron., vol. 57, no. 2, pp. 608-616, Feb. 2010.

[5] A. Kuperman, U. Levy, J. Goren, A. Zafransky, and A. Savernin, "Battery charger for electric vehicle traction battery switch station," IEEE Trans. Ind. Electron., vol. 60, no. 12, pp. 5391-5399, Dec. 2013.

[6] S. G. Li, S. M. Sharkh, F. C. Walsh, and C. N. Zhang, "Energy and battery management of a plug-in series hybrid electric vehicle using fuzzy logic," IEEE Trans. Veh. Technol., vol. 60, no. 8, pp. 3571-3585, Oct. 2011.

[7] C. H. Kim, M. Y. Kim, and G. W. Moon, "A modularized charge equalizer using a battery monitoring IC for series-connected Li-Ion battery Strings in electric vehicles," IEEE Trans. Power Electron., vol. 28, no. 8, pp. 3779-3787, May 2013.

[8] Z. Ping, Z. Jing, L.Ranran, T. Chengde, W. Qian, "Magnetic characteristics investigation of an axial-axial flux compound-structure PMSM used for HEVs," IEEE Trans. Magnetics, vol. 46, no. 6, pp. 2191- 2194, Jun. 2010.

[9] A. Kolli, O. Béthoux, A. De Bernardinis, E. Labouré, and G. Coquery, "Space-vector PWM control synthesis for an H-bridge drive in electric vehicles," IEEE Trans. Veh. Technol., vol.62, no.6, pp. 2441-2452, Jul. 2013.

[10] http://www.bluebird-electric.net/blueplanet_ecostar/solar _assisted_electric_vehicles_sustainable_transport_cars_van s.htm

[11] S. M. Yang, and J. Y. Chen, "Controlled dynamic braking for switched reluctance motor drives with a rectifier front end," IEEE Trans. Ind. Electron., vol. 60, no. 11, pp. 4913- 4919, Nov. 2013.

[12] B. Bilgin, A. Emadi, M. Krishnamurthy, "Comprehensive evaluation of the dynamic performance of a 6/10 SRM for traction application in PHEVs," IEEE Trans. Ind. Electron., vol. 60, no. 7, pp. 2564-2575, July.2013.

[13] M. Takeno, A.Chiba, N. Hoshi, S. Ogasawara, M. Takemoto, M. A. Rahman, "Test results and torque improvement of the 50-kW switched reluctance motor designed for hybrid electric vehicles," IEEE Trans. Ind. Appl., vol. 48, no. 4, pp. 1327-1334, Jul/Aug. 2012.

[14] A. Chiba, M. Takeno, N. Hoshi, M. Takemoto, S.Ogasawara, M. A. Rahman, "Consideration of number of series turns in switched-reluctance traction motor competitive to HEV IPMSM," IEEE Trans. Ind. Appl., vol. 48, no. 6, pp. 2333-2340, Nov/Dec. 2012.

[15] I. Boldea, L. N. Tutelea, L. Parsa, and D. Dorrell, "Automotive electric propulsion systems with reduced or no permanent magnets: an overview," IEEE Trans. Ind. Electron., vol. 60, no. 9, pp. 5696- 5710, Oct. 2014.